Int. J. Heat Mass Transfer. Vol. 35, No. 10, pp. 2643–2653, 1992
Printed in Great Britain

0017–9310/92 $5.00 + 0.00

Buoyancy effect on the heat convection in vertical channels with fin array at low Reynolds numbers

CHIN-HSIANG CHENG, CHEN-DON LUY and WEN-HSIUNG HUANG

Department of Mechanical Engineering, Tatung Institute of Technology,
40 Chungshan North Road Sec. 3, Taipei, Taiwan, R.O.C.

(*Received* 13 *May* 1991 *and in final form* 9 *October* 1991)

Abstract—Numerical study of the buoyancy effect on the flow pattern and heat transfer in an asymmetric-heating channel with a series of conductive fins is presented. These identical fins are attached on the relatively hotter wall at equal steamwise spaces so that a periodic flow character prevails in the fully-developed region. It is found that within one module, in addition to the typical recirculating flow at the rear of each fin, a secondary recirculating vortex appears near the colder wall when the heating of hotter wall is sufficiently intense. The strength and pattern of the secondary vortex are found to be governed by Grashof number, Reynolds number, and the geometric parameters such as fin pitch, fin height and the inclination angle of channel. Also, based on the obtained velocity and temperature solutions, the values of the pressure gradient and overall heat transfer within the solution domain are further calculated and provided. Meanwhile, buoyancy-assisted flow reversal phenomenon in the unfinned channel is also discussed and a very different feature in the flow reversal pattern between finned and unfinned channels can then be observed.

1. INTRODUCTION

CONVECTION heat transfer of flow in a parallel-plate channel with transverse fins has been a problem of great interest recently because of its practical application in heat exchangers, electronic equipment, nuclear reactors and other thermal devices. These fins can provide additional surface areas for heat transfer and improve the mixing of flow. Therefore, they are frequently used in the heat transfer augmentation techniques.

Pure forced convection in the finned channel has been studied widely. For the channel with one or a couple of fins, Durst *et al.* [1] investigated the flow separation and reattachment behavior for various Reynolds numbers. Cheng and Huang [2] evaluated the effect of fins on developing flow when the fins are placed in the entrance region, and presented numerical results of local heat transfer and friction loss.

When the number of fins in the channel is increased, a streamwise-periodic flow pattern may be approximately developed after sufficient distance for development. That is, if the region between two successive fins is considered, the outflow profiles will become nearly the same as the inflow profiles. This pattern was observed experimentally by Berner *et al.* [3]. On the other hand, for analysing this periodically fully-developed flow, a theoretical background was provided by Patankar *et al.* [4]. Based on the concepts described in ref. [4], many authors, such as Webb and Ramadhyani [5], Kelkar and Patankar [6], and Cheng and Huang [7], have further investigated the pure forced convection problems in the parallel-plate channel with fin arrays.

The validity of the above forced-convection analyses [2–7] is restricted to the cases of very high flow velocity or slight wall heating in which the effect of buoyancy force can be neglected. However, if the wall heating is sufficiently strong or the flow velocity slow, the effect of buoyancy force will be appreciable and needs to be taken into account in the mathematical model.

As a matter of fact, increasing attention has been focused on a buoyancy-induced flow reversal phenomenon in the unfinned smooth channels. Considering the smooth vertical channels with asymmetric wall temperatures, Aung and Worku [8, 9] presented the numerical solution for developing flow and the analytical solution for fully-developed flow as well. They found that when the wall heating is sufficiently intense, flow reversal can occur near the relatively colder wall in a buoyancy-assisted situation. The developing flow with flow reversal was further studied by Ingham *et al.* [10]. A FLARE-like marching procedure was employed in ref. [10] to forward the numerical calculation from inlet to fully-developed region where reversed flow may occur. Cheng *et al.* [11] extended and solved the fully-developed problems by considering more thermal boundary conditions, and parameter zones for the occurrence of reversed flow under various boundary conditions were found.

According to these previous studies, it is recognized that the existence of fins in a channel interrupts the flow field and hence, results in a remarkable change

NOMENCLATURE

B	body force
D_h	hydraulic diameter
d	pitch length of fin array
e	fin height
f_p	pressure gradient factor
Gr	Grashof number
g	gravitational acceleration
H	channel width
P	dimensionless fluid pressure
Pr	Prandtl number
p	fluid pressure
$\tilde{p}$	periodic variation part of pressure
p_0	reference pressure
Q	overall heat transfer in one module
Q_x	dimensionless local heat flux on wall
Q_{fy}	dimensionless local heat flux on fin surface
Re	Reynolds number
T	fluid temperature
U	dimensionless fluid velocity in x-direction
u	fluid velocity in x-direction
u_m	average axial velocity
V	dimensionless fluid velocity in y-direction
v	fluid velocity in y-direction
W	dimensionless fluid vorticity
w	fluid vorticity
X, Y	dimensionless coordinate system
x, y	rectangular coordinate system.

Greek symbols

α	thermal diffusivity of fluid
β	coefficient of volumetric expansion of fluid
θ	dimensionless fluid temperature
ν	kinematic viscosity of fluid
ρ	fluid density
τ	global pressure gradient
ψ	dimensionless stream function
φ	stream function
ϕ	inclination angle of channel.

Subscripts

0	pure forced convection in smooth channel
1	hotter wall
2	colder wall.

in flow pattern. It is also known that such a flow pattern may be further altered by the buoyancy effect. Inasmuch as the buoyancy has a profound influence on flow reversal and thermal characteristics in unfinned channels [8–11], it is expected that in a finned channel the influence of buoyancy is likewise appreciable and worthy of investigation. However, even though the heat transfer in a finned channel has so far been studied extensively (e.g. refs. [1–7]), the information of this mixed-convection flow is still lacking.

Therefore, the present study performed the numerical calculation to evaluate the buoyancy effect on the laminar, periodically fully-developed flow in vertical channels with fin array. Various physical arrangements are considered in order to evaluate their influence on heat transfer and pressure drop.

A vertical parallel-plate channel with fin array mounted on the hotter wall is shown in Fig. 1. A series of fins of equal height (e) are spaced on the hotter wall at equal streamwise space (d) so that a periodic flow character is developed. Hence, one may calculate the flow and temperature fields in a unit module with no need of computation for the entrance region. The channel walls are maintained with uniform but not equal surface temperatures. Also, the fins mounted on hotter wall are assumed to be perfectly conductive so that the surface temperature of each fin is uniform and equal to the temperature of the hotter wall.

The magnitude of buoyancy force is denoted quantitatively by Grashof number (Gr). Basically, flow behavior is governed by Reynolds number, Grashof number, and the geometric parameters such as fin pitch (d/H), fin height (e/H) and inclination angle of channel (ϕ). Since the effect of buoyancy force becomes particularly appreciable in the low Reynolds number cases, only the results of $Re \leqslant 500$ are presented. Grashof number is up to 10^5, and the regions

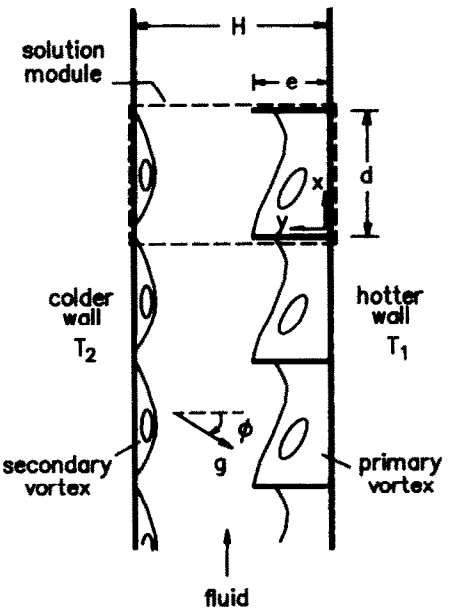

FIG. 1. A vertical parallel-plate channel with fin array.

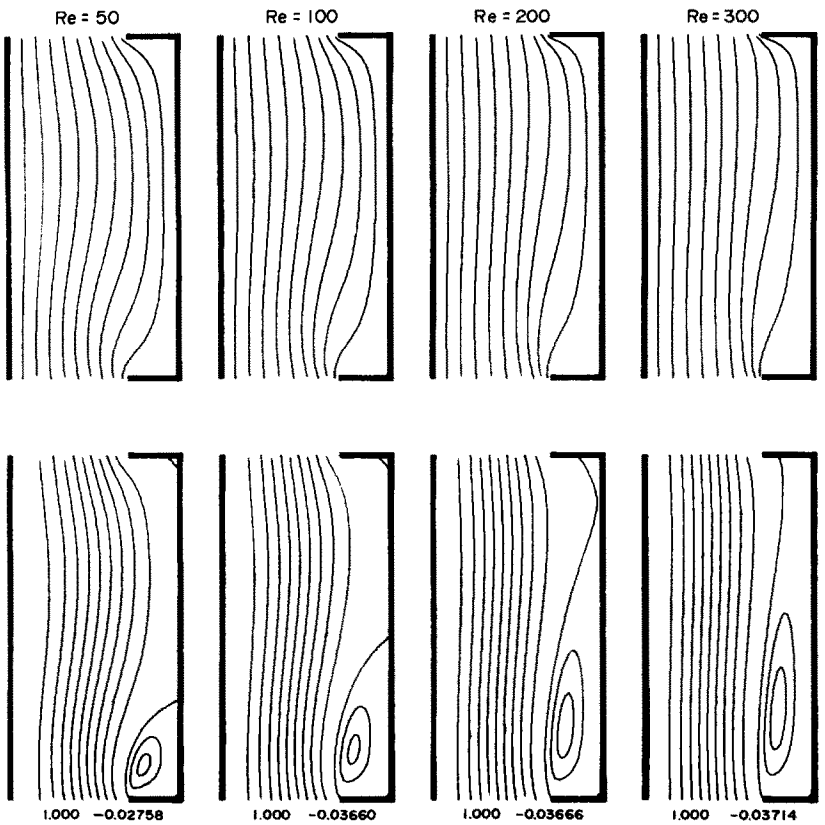

FIG. 2. Effect of Reynolds number on flow pattern and temperature distribution for $d/H = 2$, $e/H = 0.3$ and $Gr = 10^4$.

of fin pitch and fin height are considered to be within $1 \leqslant d/H \leqslant 7$ and $0 \leqslant e/H \leqslant 0.5$, respectively.

It is noted that when the fin pitch is arranged to be very large, the influence of fins on the flow will be negligible; therefore, the channel can be treated as an unfinned smooth channel. On the other hand, as the pitch of fins approaches zero, the connected fins construct a nearly continuous solid surface so that the channel can be treated as another smooth but narrower channel (with width of $H-e$). The analytical solutions for these two limiting cases can be deduced from the solutions of ref. [9], and will be provided later for comparison with the numerical results.

The channel is mainly arranged to stand vertically ($\phi = 90°$). Fluid flow goes upwards and is heated by the walls, subject to a buoyancy-assisted situation. Since the inclination angle is another influential factor to the flow, the results of $0° \leqslant \phi \leqslant 180°$ are also presented in this study to illustrate the angle effect. However, for cases of $180° \leqslant \phi \leqslant 360°$ in which the flow goes down but is still heated by the wall, the flow becomes a buoyancy-opposed flow. In these cases fluid velocity is retarded by the opposing buoyancy so that heat transfer may be reduced. Thus, cases of $180° \leqslant \phi \leqslant 360°$ are not considered herein because of practical application.

Besides, the Prandtl number of fluid is also an important factor influencing the flow and thermal fields. A higher Prandtl number always produces higher heat transfer rate, as already discussed in refs. [5–7]. In this study, the value of Prandtl number is fixed at 0.71 for air flow without consideration of Prandtl number effect.

2. ANALYSIS

2.1. *Governing equations*

The flow and temperature fields are assumed to be two-dimensional and laminar with constant properties, except the variation of density in the buoyancy term of momentum equation. The density variation is treated by the Boussinesq approximation. Thus, the continuity, momentum and energy equations governing the flow in channel are

$$\frac{\partial u}{\partial x} + \frac{\partial v}{\partial y} = 0 \tag{1}$$

$$u\frac{\partial u}{\partial x} + v\frac{\partial u}{\partial y} = -\frac{1}{\rho}\frac{\partial p}{\partial x} + \nu\left(\frac{\partial^2 u}{\partial x^2} + \frac{\partial^2 u}{\partial y^2}\right) - B_x \tag{2}$$

$$u\frac{\partial v}{\partial x} + v\frac{\partial v}{\partial y} = -\frac{1}{\rho}\frac{\partial p}{\partial y} + \nu\left(\frac{\partial^2 v}{\partial x^2} + \frac{\partial^2 v}{\partial y^2}\right) - B_y \tag{3}$$

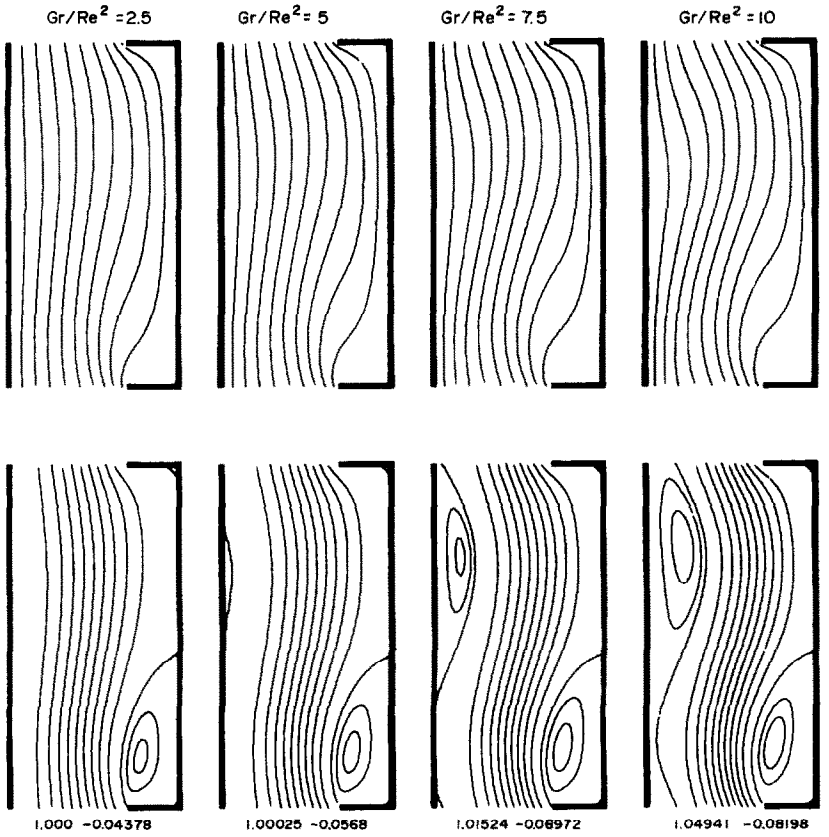

FIG. 3. Buoyancy effect on flow pattern and temperature distribution for $d/H = 2$, $e/H = 0.3$ and $Re = 100$.

$$u\frac{\partial T}{\partial x} + v\frac{\partial T}{\partial y} = \alpha\left(\frac{\partial^2 T}{\partial x^2} + \frac{\partial^2 T}{\partial y^2}\right). \tag{4}$$

If the channel is inclined with angle ϕ from the horizontal plane, the body force terms in the momentum equations are expressed by $B_x = \rho g \sin\phi$ and $B_y = \rho g \cos\phi$. Accordingly, for the vertical-channel cases ($\phi = 90°$), one has $B_x = \rho g$ and $B_y = 0$.

The periodic conditions, as given in refs. [4–7], are

$$u(x, y) = u(x+d, y) \tag{5a}$$

$$v(x, y) = v(x+d, y) \tag{5b}$$

$$p(x, y) = -\tau x + \bar{p}(x, y)$$

$$\text{with } \bar{p}(x, y) = \bar{p}(x+d, y) \tag{5c}$$

$$T(x, y) = T(x+d, y). \tag{5d}$$

In equation (5c), the term τx accounts for the global pressure drop and hence, $-\tau$ denotes the pressure gradient. The quantity $\bar{p}(x, y)$ is the periodic variation term.

The primitive variable equations (1)–(4), will not be solved directly. Instead, as discussed in ref. [7], the stream function–vorticity method is adopted in this study to solve these equations. The dimensionless formulation of the stream function–vorticity method can be derived by defining the dimensionless stream function and vorticity with

$$U = \frac{\partial \psi}{\partial Y}, \quad V = -\frac{\partial \psi}{\partial X} \tag{6}$$

and

$$W = \frac{\partial V}{\partial X} - \frac{\partial U}{\partial Y} \tag{7}$$

respectively. One obtains

$$U\frac{\partial W}{\partial X} + V\frac{\partial W}{\partial Y} = \frac{2}{Re}\left(\frac{\partial^2 W}{\partial X^2} + \frac{\partial^2 W}{\partial Y^2}\right) + \frac{1}{2}\left(\frac{Gr}{Re^2}\right)\left(\frac{\partial \theta}{\partial X}\cos\phi - \frac{\partial \theta}{\partial Y}\sin\phi\right) \tag{8}$$

$$\frac{\partial^2 \psi}{\partial X^2} + \frac{\partial^2 \psi}{\partial Y^2} = -W \tag{9}$$

$$U\frac{\partial \theta}{\partial X} + V\frac{\partial \theta}{\partial Y} = \frac{2}{Re\,Pr}\left(\frac{\partial^2 \theta}{\partial X^2} + \frac{\partial^2 \theta}{\partial Y^2}\right) \tag{10}$$

where the dimensionless parameters are

$$X = x/H, \quad Y = y/H, \quad U = u/u_m, \quad V = v/u_m,$$

$$\psi = \varphi/(u_m H), \quad W = wH/u_m,$$

$$\theta = (T - T_2)/(T_1 - T_2), \quad Pr = \nu/\alpha.$$

u_m refers to the average axial velocity, and Prandtl number is assigned to be 0.71 here for air flow. The

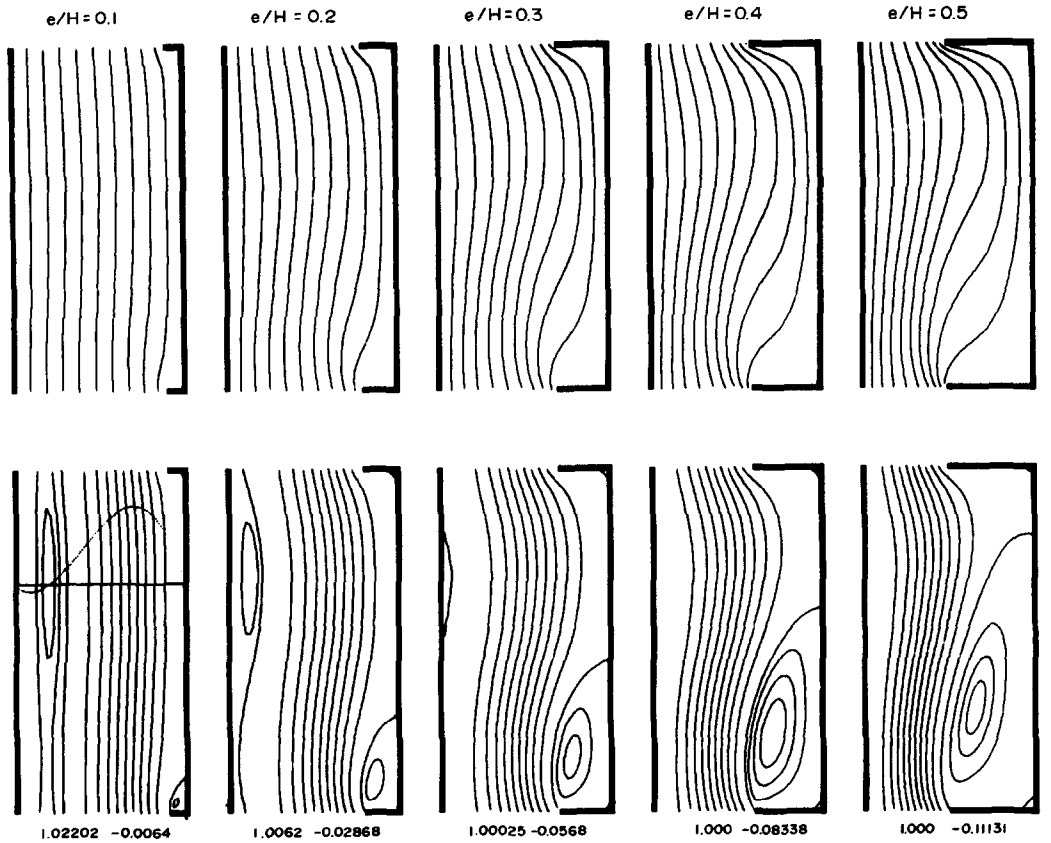

FIG. 4. Effect of fin height on flow pattern and temperature distribution for $d/H = 2$, $Re = 100$ and $Gr = 5 \times 10^4$.

Reynolds number and Grashof number are defined, respectively, by

$$Re = u_m D_h / \nu \tag{11a}$$

and

$$Gr = g\beta(T_1 - T_2)D_h^3/\nu^2. \tag{11b}$$

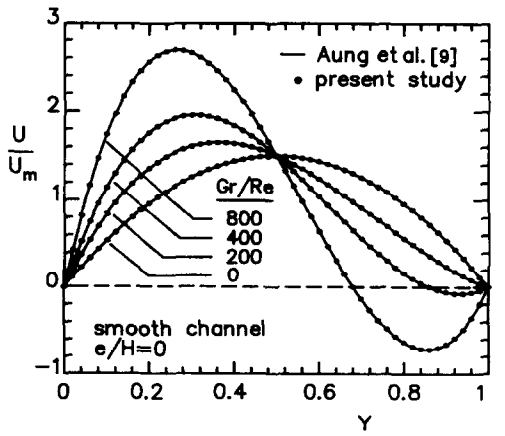

FIG. 5. Reversed flow profiles of unfinned smooth channels.

In the previous expressions, D_h refers to the hydraulic diameter of the channel.

The boundary conditions at the upstream and downstream faces of the solution domain are given with $\psi(0, Y) = \psi(d/H, Y)$, $W(0, Y) = W(d/H, Y)$ and $\theta(0, Y) = \theta(d/H, Y)$. Note that the periodic behavior still holds for the stream function and vorticity, based on the definitions of equations (5)–(7). And the conditions on the solid surfaces are

$$U = 0, \quad V = 0, \quad \psi = 0, \quad W = -\frac{\partial^2 \psi}{\partial N^2},$$

$$\theta = 1 \quad \text{on the hotter wall and fin surfaces;} \tag{12a}$$

and

$$U = 0, \quad V = 0, \quad \psi = 1, \quad W = -\frac{\partial^2 \psi}{\partial N^2},$$

$$\theta = 0 \quad \text{on the colder wall surface} \tag{12b}$$

where N represents the normal-direction coordinate of the related solid surface.

Once U and V have been obtained, the global pressure gradient can be further calculated with the dimensionless momentum equation in the x-direction

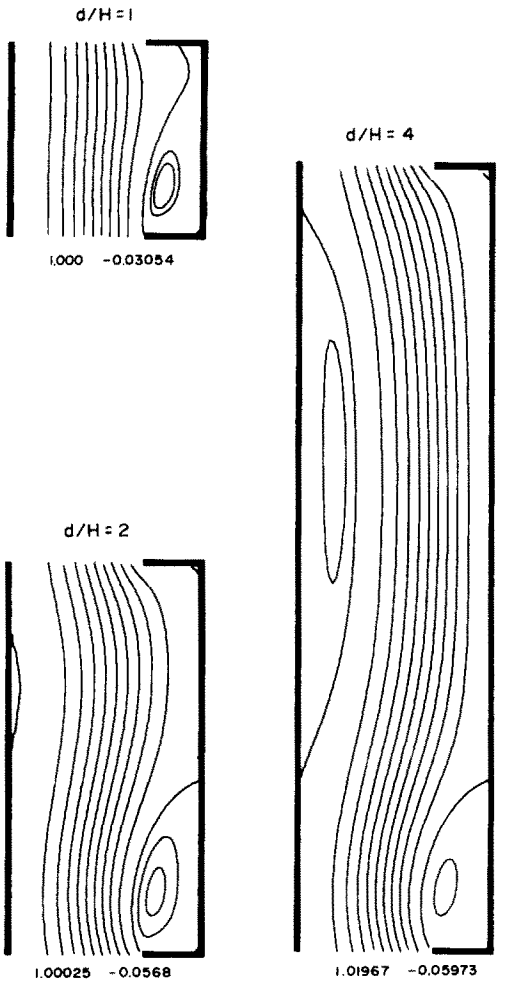

FIG. 6. Flow patterns for various pitch lengths, with $e/H = 0.3$, $Re = 100$ and $Gr = 5 \times 10^4$.

$$\frac{f_p}{4} - \frac{\partial P}{\partial X} = U\frac{\partial U}{\partial X} + V\frac{\partial U}{\partial Y} - \frac{2}{Re}\left(\frac{\partial^2 U}{\partial X^2} + \frac{\partial^2 U}{\partial Y^2}\right) - \frac{\theta}{2}\left(\frac{Gr}{Re^2}\right)\sin\phi \quad (13)$$

where $P = (\bar{p} - p_0)/(\rho u_m^2)$ and p_0 is a reference pressure. The value of f_p, indicating global pressure gradient, is termed 'pressure gradient factor' in this study and defined by

$$f_p = \tau D_h/(\tfrac{1}{2}\rho u_m^2). \quad (14)$$

By applying the periodic conditions of P on the upstream and downstream faces, the pressure gradient factor can be calculated through the integration of equation (13) along the axial direction between two corresponding points on the respective faces, following [7] in derivation, that is

$$f_p = 4(H/d)\int_0^{d/H}\left[U\frac{\partial U}{\partial X} + V\frac{\partial U}{\partial Y} - \frac{2}{Re}\left(\frac{\partial^2 U}{\partial X^2} + \frac{\partial^2 U}{\partial Y^2}\right) - \frac{\theta}{2}\left(\frac{Gr}{Re^2}\right)\sin\phi\right]dX. \quad (15)$$

It is noted that f_p approaches to the friction factor defined in the pure forced convection analyses [5–7] as Grashof number diminishes to zero.

On the other hand, the solution of temperature distribution enables the heat transfer performance to be further evaluated. The dimensionless local heat flux on wall (Q_x) is defined by

$$Q_x = -\frac{H}{T_1 - T_2}\frac{\partial T}{\partial y}\bigg|_{wall}. \quad (16a)$$

The dimensionless local heat flux from the fin surfaces (Q_{fy}) is given by

$$Q_{fy} = \pm\frac{H}{T_1 - T_2}\frac{\partial T}{\partial x}\bigg|_{fin} \quad (16b)$$

where the signs '+' and '−' are selected for the left and right surfaces of fin, respectively.

Thus, the overall heat transfer (Q) from hotter wall to colder wall within one module can be calculated by the integration of Q_x along the colder wall from $X = 0$ to $X = d/H$, i.e.

$$Q = \int_0^{d/H} Q_x\,dX, \quad \text{along the colder wall.} \quad (17)$$

2.2. *Numerical methods*

By means of an iterative finite difference scheme similar to that used in refs. [2, 7], solutions of ψ, W, θ, U and V are carried out by solving equations (6)–(10) numerically. The finite difference expressions of vorticity transport equation (8) and energy equation (10) are obtained by taking volume integration over discrete cells surrounding the grid points and solved iteratively by the alternating direction implicit method (ADI). Meanwhile, the successive over-relaxation method (SOR) is applied to the equation of stream function (9). A grid system of 101×51 grid points is adopted typically in this computation after a careful check for the grid-independence of the numerical solution. The detailed information of the numerical procedure, which will not be described further, can be found in refs. [2, 7].

2.3. *Limiting cases with very large or very small fin pitch*

2.3.1. *Very large fin pitch* ($d/H \to \infty$). As discussed in the foregoing section, when the pitch length of fins approaches infinity, the influence of fins on the flow becomes slight. Hence, the solutions go to those of the unfinned smooth channel. Based on the velocity and temperature profiles provided by Aung and Worku [9], the pressure gradient factor and overall heat transfer within a module length ($0 \leqslant X \leqslant d/H$) in the smooth channel can be derived readily as

$$f_p Re = 96 - Gr/Re \quad (18a)$$

$$Q = d/H. \quad (18b)$$

The obtained numerical solutions of the present study

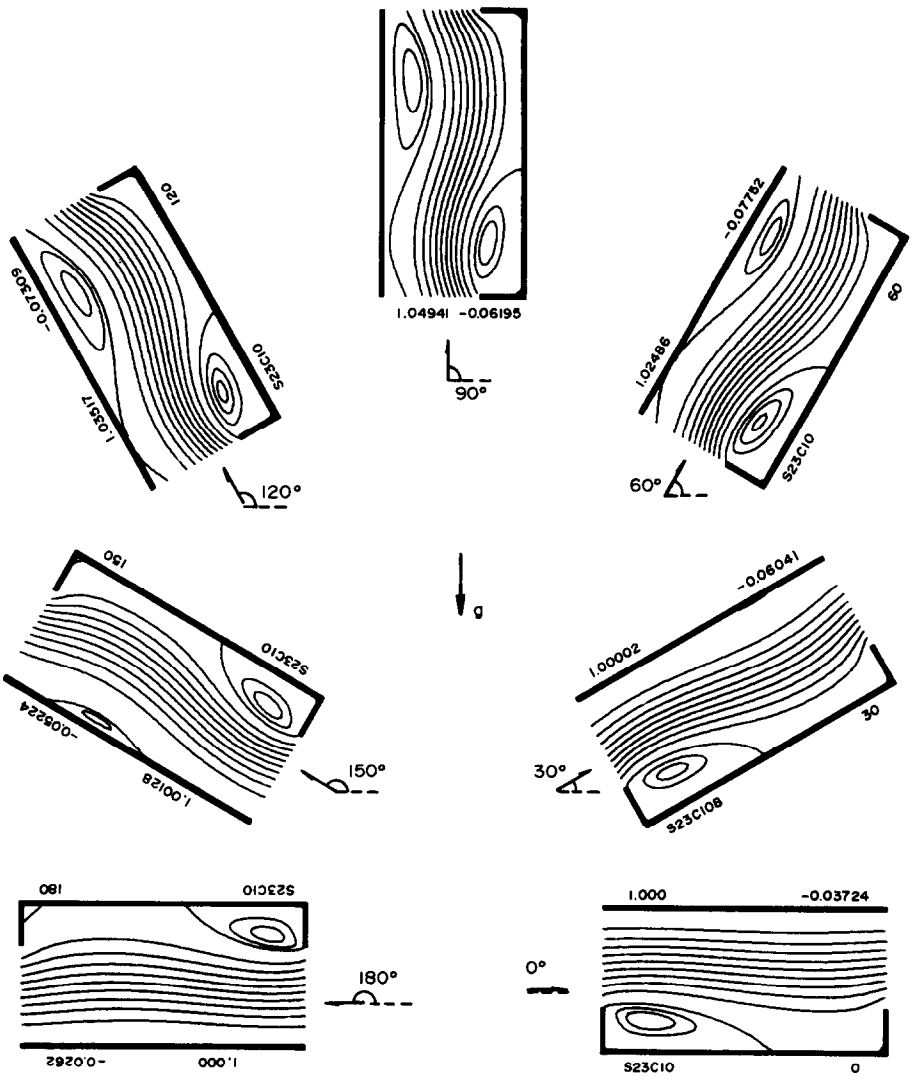

FIG. 7. Variation of flow pattern with inclination angle for $d/H = 2$, $e/H = 0.3$, $Re = 100$ and $Gr = 10^5$.

can match accurately the analytical solutions described by equation (18). Their agreement will be shown later.

2.3.2. *Very small fin pitch* ($d/H \to 0$). On the contrary, when the pitch approaches zero, the channel can be treated as another smooth but narrower channel, i.e. a smooth channel with width of $H-e$. For this limiting case, one can have

$$f_p Re = 96/[1-(e/H)]^3 - Gr/Re \qquad (19a)$$

$$Q = (d/H)/[1-(e/H)]. \qquad (19b)$$

3. RESULTS AND DISCUSSION

3.1. *Flow and temperature fields*

Figure 2 shows the effect of Reynolds number on flow pattern and temperature field in a vertical channel for the case of $d/H = 2$, $e/H = 0.3$ and $Gr = 10^4$. The values given at the bottom of each diagram indicate the maximum and minimum stream functions. It is seen that as the Reynolds number varies from 50 to 300, the size as well as the strength of the recirculating vortex at the rear of fin apparently increases. The space between two fins is occupied entirely by the vortex once Re is up to 200. However, it is found that the Reynolds number seemingly has slighter influence on temperature field than on velocity field.

The buoyancy effect on the flow pattern and temperature distribution is shown in Fig. 3. For the case of $d/H = 2$, $e/H = 0.3$ and $Re = 100$, a remarkable change in flow pattern caused by the increase of Grashof number can be observed. It is noticed that as the ratio Gr/Re^2 is raised up to 5, a secondary recirculating vortex near the colder wall starts to develop and it grows rapidly as Gr/Re^2 continues to increase. The reason for the occurrence of the sec-

ondary vortex may be attributed to a positive streamwise pressure gradient developed in the channel which opposes inertial and buoyancy forces and supports the secondary vortex. The value of the pressure gradient will be given and discussed in the next section.

Figure 4 illustrates the effect of fin height for $d/H = 2$, $Re = 100$ and $Gr = 5 \times 10^4$. It is interesting to find that as fins become higher the primary vortex grows remarkably, whereas the secondary vortex gradually disappears. In Fig. 4, for $e/H = 0.1$, a dotted curve is provided to display the velocity profile at the cross-section passing through the secondary vortex. It is noticed that if e/H is decreased to zero, the velocity profile exactly goes to the fully reversed flow profiles of the unfinned smooth channel considered in refs. [8–11]. This certainly provides a test for the validity and accuracy of the numerical method. The comparison between the present numerical data and the theoretical solutions provided by Aung *et al.* [9] for various values of Gr/Re is shown in Fig. 5. And an excellent agreement has been found.

For $e/H = 0.3$, $Re = 100$ and $Gr = 5 \times 10^4$, the influence of pitch length on the flow is illustrated in Fig. 6. It is obvious that the larger fin pitch is more encouraging to the secondary vortex motion. As d/H approaches infinity, the velocity distribution asymptotically goes to the smooth-channel solution for $Gr/Re = 500$ in ref. [9].

Aside from these physical and geometric parameters introduced above, the inclination angle of the channel is an influential factor that may affect the recirculating flow pattern and heat transfer. Figure 7 shows the effect of inclination angle on the flow, for $d/H = 2$, $e/H = 0.3$, $Re = 100$ and $Gr = 10^5$. One may expect that as ϕ varies from 0° to 180°, the buoyancy force will be strongest at vertical arrangement ($\phi = 90°$) and weakest at horizontal situations ($\phi = 0°$ and $\phi = 180°$). Actually, in this figure the stronger secondary vortex can really be seen at angle closer to 90°. Note that flow patterns of ϕ varying from 90° to 0° are different from those of ϕ varying from 90° to 180°.

3.2. *Heat transfer and pressure drop*

Attention is drawn to the heat transfer characteristics and pressure gradient. The results of overall heat transfer and pressure drop are presented with the ratios of finned-channel values to the values associ-

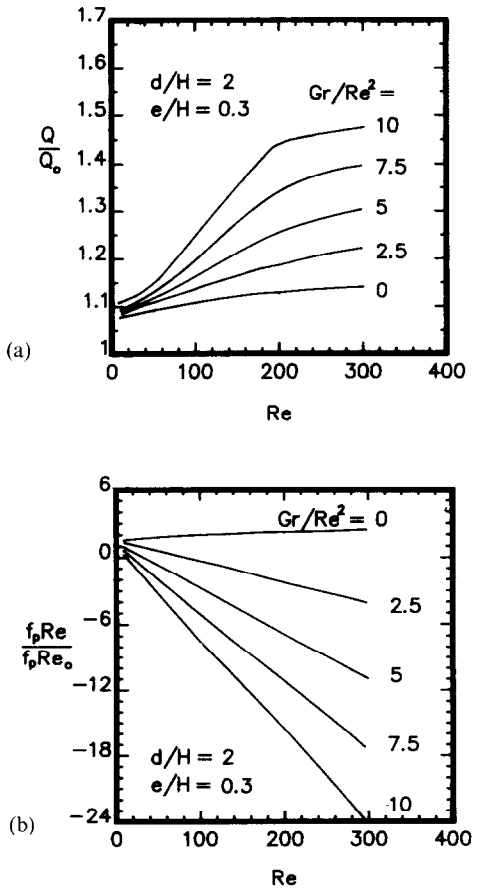

FIG. 8. Variation of overall heat transfer and pressure gradient factor with Reynolds number for $d/H = 2$ and $e/H = 0.3$: (a) Q/Q_0–Re; (b) f_pRe/f_pRe_0–Re.

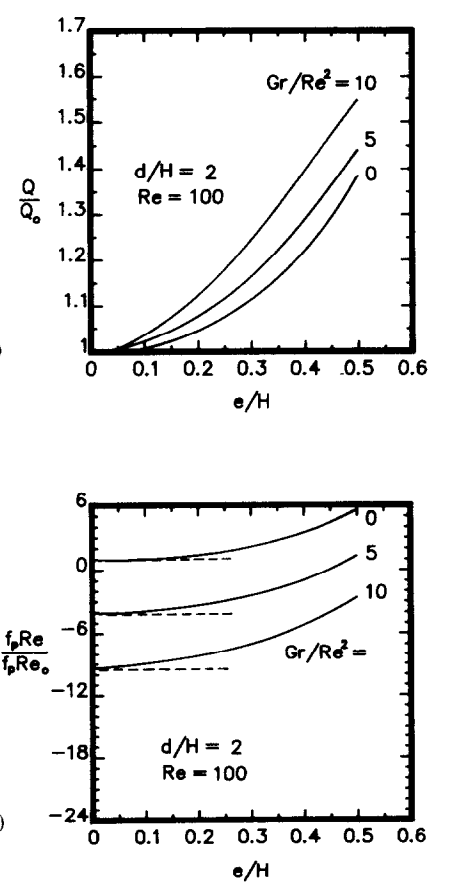

FIG. 9. Variation of overall heat transfer and pressure gradient factor with fin height for $d/H = 2$ and $Re = 100$: (a) Q/Q_0–e/H; (b) f_pRe/f_pRe_0–e/H.

ated with forced convection in unfinned channel (i.e. with Q/Q_0 and f_pRe/f_pRe_0). The values of Q_0 and f_pRe_0 are equal to d/H and 96, respectively, from equation (18) by letting $Gr = 0$. The same values can also be obtained readily using the information provided by Shah and London [12].

Figure 8 shows the variations of overall heat transfer and pressure gradient with Reynolds number for $d/H = 2$ and $e/H = 0.3$. It is noted that the curves of $Gr/Re^2 = 0$ denote the data of pure forced convection. An increase of 50% in heat transfer can be observed on the curve of $Gr/Re^2 = 10$ as Re reaches 300. On the other hand, it is noticed that the value of f_pRe/f_pRe_0 is always positive for $Gr/Re^2 = 0$. However, as Gr/Re^2 is elevated, the pressure gradient factor may become negative. This implies a positive streamwise pressure gradient prevailing in the channel. As stated earlier, such a positive pressure gradient produces a force in reverse direction against the buoyancy and inertial forces and supports the occurrence of the secondary vortex.

The effect of fin height on overall heat transfer and pressure gradient factor is illustrated in Fig. 9. Higher fins are employed to provide more heat transfer areas. Hence, in Fig. 9(a), overall heat transfer increases significantly with e/H. Note that $e/H = 0$ represents the smooth channel case in which Q/Q_0 becomes unity and f_pRe/f_pRe_0 can be calculated with

$$f_pRe/f_pRe_0 = 1 - Gr/(96Re). \tag{20}$$

The values of f_pRe/f_pRe_0 for $e/H = 0$ obtained with the above equation for various values of Gr/Re^2 are indicated by dashed lines in Fig. 9(b). The good agreement between the numerical solutions of very small e/H and the theoretical solutions can be seen.

Figures 10(a) and (b) show the influence of pitch length on the heat transfer and pressure gradient, respectively, under various Reynolds numbers for $Gr/Re^2 = 5$ and $e/H = 0.3$. The heat transfer exhibits a remarkable change along with the variation of pitch length, especially for higher Reynolds number cases. But the pressure gradient is merely slightly affected by the pitch length. Since the channel with $d/H \to 0$ approaches a smooth but narrower channel, the values of Q/Q_0 and f_pRe/f_pRe_0 for small d/H are expressed with

$$Q/Q_0 = 1/[1 - (e/H)] \tag{21a}$$

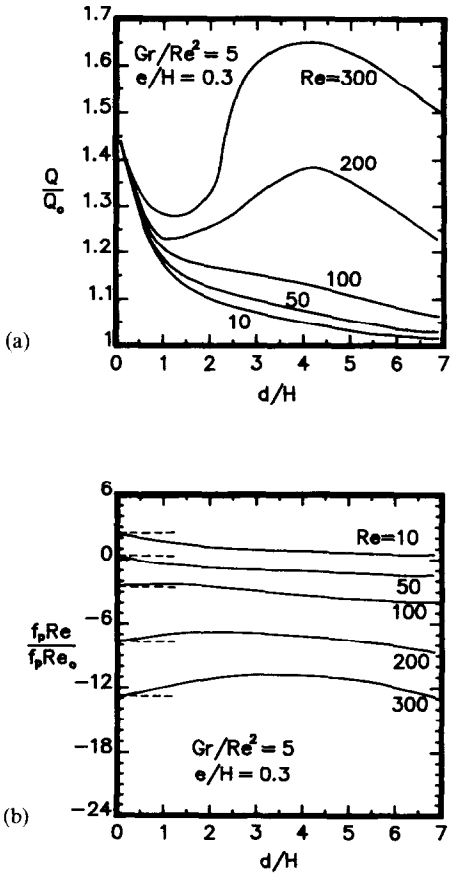

FIG. 10. Variation of overall heat transfer and pressure gradient factor with fin pitch for $e/H = 0.3$ and $Gr/Re^2 = 5$: (a) Q/Q_0–d/H; (b) f_pRe/f_pRe_0–d/H.

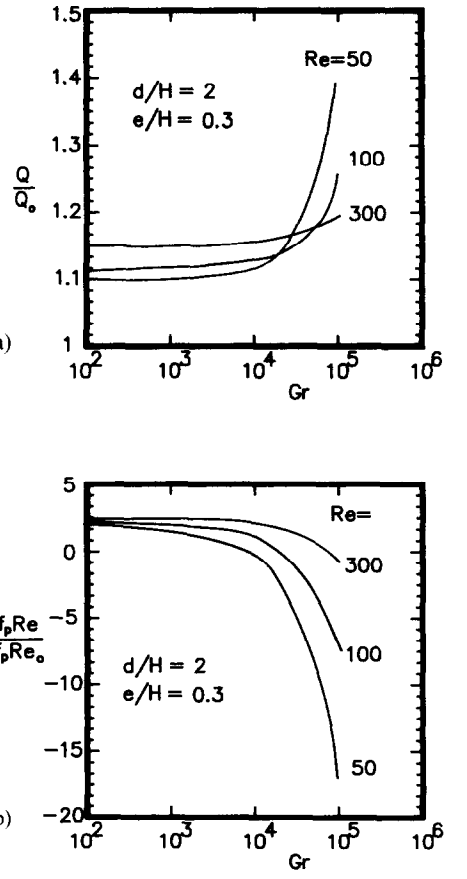

FIG. 11. Variation of overall heat transfer and pressure gradient factor with Grashof number for $d/H = 2$ and $e/H = 0.3$: (a) Q/Q_0–Gr; (b) f_pRe/f_pRe_0–Gr.

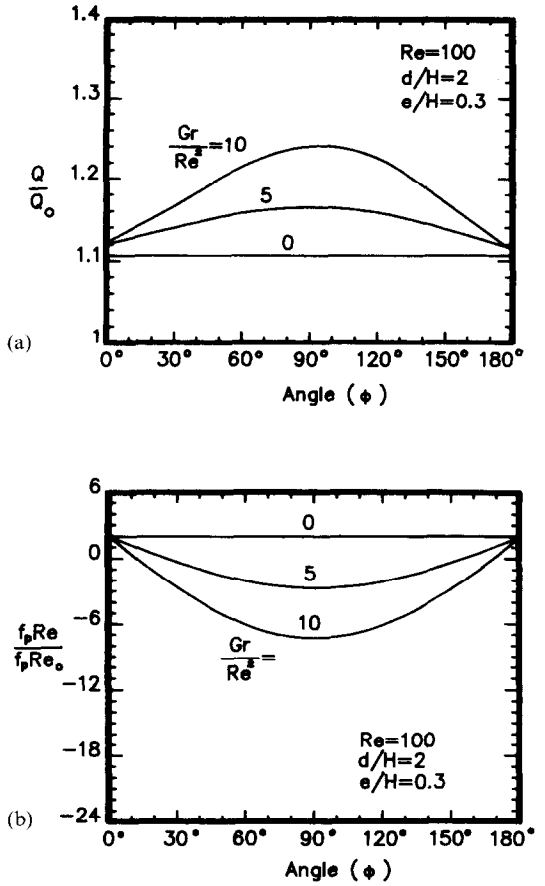

FIG. 12. Effect of inclination angle on overall heat transfer and pressure gradient for $d/H = 2$, $e/H = 0.3$ and $Re = 100$: (a) Q/Q_0–ϕ; (b) f_pRe/f_pRe_0–ϕ.

and

$$f_pRe/f_pRe_0 = 1/[1-(e/H)]^3 - Gr/(96Re) \quad (21b)$$

respectively. According to the previous equations, one may have $Q/Q_0 = 1/0.7 = 1.43$ at $d/H = 0$ for the present case. Note that this value is independent of the Reynolds number. And in Fig. 10(a), it is clear that the numerical solutions accurately satisfy this limiting condition.

The theoretical values of f_pRe/f_pRe_0 calculated from equation (21b) for $d/H = 0$ under various Reynolds numbers are displayed with dashed lines in Fig. 10(b). A good agreement between the numerical solutions and the theoretical solutions is also found.

The buoyancy effect may be properly illustrated in Fig. 11. For $d/H = 2$ and $e/H = 0.3$, Fig. 11(a) provides the variation of overall heat transfer with Grashof number under various Re values. It is found that only for a Grashof number less than approximately 10^4 is the heat transfer accurately predicted by the pure forced convection estimate. For Gr higher than 10^4, the buoyancy effect becomes relatively important and should be taken into account in the mathematical model. Normally, the lower Reynolds number cases experience more significant variations as Gr is increased. The results of pressure gradient factor are shown in Fig. 11(b).

Figure 12 shows the dependence of heat transfer and pressure gradient on inclination angle. As already observed in Fig. 7, the influence of buoyancy force is strongest in the vertical arrangement. Therefore, one may find that the curves in Fig. 12(a) reach maximum values, and those in Fig. 12(b) reach minimum values, at $\phi = 90°$. In general, the flows of higher Gr/Re^2 have greater dependence on the inclination angle.

4. CONCLUSIONS

Numerical study of the buoyancy effect on heat convection of the periodically fully-developed flow in a vertical channel with a series of fins has been performed. Results of various physical parameters are presented to show the influence of buoyancy force, at low Reynolds numbers, on flow pattern and thermal characteristics. In general, a primary vortex is found at the rear of each fin. However, if hotter wall heating is sufficiently strong, a positive pressure gradient is formed within the channel and then a series of buoyancy-induced secondary vortices may appear, one in each module, near the colder wall. The occurrence of this secondary vortex is governed by the Grashof number, the Reynolds number, and the geometric parameters such as fin pitch, fin height and inclination angle of channel.

When the fin height (e/H) becomes zero, the present numerical solution of velocity accurately matches the theoretical solutions presented by refs. [8–11] for a smooth channel. Meanwhile, for the cases of very large and very small fin pitches (d/H), the numerical results of the pressure gradient factor and overall heat transfer also reasonably approach the theoretical values given by equations (18) and (19).

Results for a typical case show that only for a Grashof number less than approximately 10^4 is the heat transfer accurately predicted by the pure forced convection estimate. For Gr higher than 10^4, the buoyancy effect becomes appreciable and hence, it should be taken into account in the mathematical model. The buoyancy effect on the flow is the strongest when the channel is arranged to be vertical. Meanwhile, the overall heat transfer increases with the fin height and the Reynolds number.

REFERENCES

1. F. Durst, M. Founti and S. Obi, Experimental and computational investigation of the two-dimensional channel flow over two fences in tandem, *J. Fluids Engng* **110**, 48–54 (1988).
2. C. H. Cheng and W. H. Huang, Laminar forced convection flows in horizontal channels with transverse fins placed in entrance regions, *Numer. Heat Transfer A* **16**, 77–100 (1989).
3. C. Berner, F. Durst and D. M. McEligot, Flow around baffles, *J. Heat Transfer* **106**, 743–749 (1984).
4. S. V. Patankar, C. H. Liu and E. M. Sparrow, Fully developed flow and heat transfer in ducts having stream-

wise-periodic variations of cross-sectional area, *J. Heat Transfer* **99,** 180–186 (1977).
5. B. W. Webb and S. Ramadhyani, Conjugate heat transfer in a channel with staggered ribs, *Int. J. Heat Mass Transfer* **28,** 1679–1687 (1985).
6. K. M. Kelkar and S. V. Patankar, Numerical prediction of flow and heat transfer in a parallel plate channel with staggered fins, *J. Heat Transfer* **109,** 25–30 (1987).
7. C. H. Cheng and W. H. Huang, Numerical prediction for laminar forced convection in parallel-plate channels with transverse fin arrays, *Int. J. Heat Mass Transfer* **34,** 2739–2749 (1991).
8. W. Aung and G. Worku, Developing flow and flow reversal in a vertical channel with asymmetric wall temperatures, *J. Heat Transfer* **108,** 299–304 (1986).
9. W. Aung and G. Worku, Theory of fully developed, combined convection including flow reversal, *J. Heat Transfer* **108,** 485–488 (1986).
10. D. B. Ingham, D. J. Keen and P. J. Heggs, Flows in vertical channels with asymmetric wall temperatures and including situations where reverse flows occur, *J. Heat Transfer* **110,** 910–917 (1988).
11. C. H. Cheng, H. S. Kou and W. H. Huang, Flow reversal and heat transfer of fully developed mixed convection in vertical channels, *AIAA J. Thermophys. Heat Transfer* **4,** 375–383 (1990).
12. R. K. Shah and A. L. London, Laminar flow forced convection in ducts. In *Advances in Heat Transfer* (Edited by T. F. Irvine and J. P. Hartnett), Supplement 1, pp. 153–189. Academic Press, New York (1978).

EFFET DE FLOTTEMENT SUR LA CONVECTION THERMIQUE DANS DES CANAUX VERTICAUX AVEC PICOTS A FAIBLE NOMBRE DE REYNOLDS

Résumé—On présente l'étude numérique de l'effet de flottement sur la configuration d'écoulement et le transfert thermique dans un canal chauffé axisymétriquement et avec une série de picots conductifs. Ceux-ci sont identiques, attachés à la paroi plus chaude avec des espacements égaux dans le sens de l'écoulement de façon que s'établisse une région avec un écoulement périodique. On trouve que dans un module, en plus de l'écoulement typique de recirculation à l'arrière de chaque picot, un vortex secondaire apparaît près de la paroi froide quand le chauffage de la paroi chaude est suffisamment intense. L'intensité et la configuration du vortex sont trouvés être gouvernées par le nombre de Grashof, le nombre de Reynolds et les paramètres géométriques tels que le pas entre picots, la hauteur des picots et l'angle d'inclinaison du canal. A partir de solutions de vitesse et de température obtenues, les valeurs du gradient de pression et du transfert thermique global sont calculées. On discute aussi le phénomène de renversement de l'écoulement dû au flottement, dans le canal sans picots. On observe une configuration très différente dans l'écoulement de retour entre les canaux avec ou sans picots.

AUFTRIEBSEINFLÜSSE AUF DIE KONVEKTIVE WÄRMEÜBERTRAGUNG IN SENKRECHTEN KANÄLEN MIT RIPPENANORDNUNGEN BEI KLEINER REYNOLDS-ZAHL

Zusammenfassung—Der Auftriebseinfluß auf das Strömungsfeld und den Wärmeübergang in einem asymmetrisch beheizten Kanal mit einer Reihe von wärmeleitenden Rippen wird numerisch untersucht. Diese identischen Rippen sind an der vergleichsweise wärmeren Wand mit in Strömungsrichtung gleichmäßigen Abständen angebracht, so daß im Gebiet vollständig ausgebildeter Strömung ein periodischer Charakter vorherrscht. Es zeigt sich, daß innerhalb eines Moduls zusätzlich zu der typischen Rezirkulationsströmung im Nachlauf jeder Rippe ein sekundärer Rezirkulationswirbel in der Nähe der kälteren Wand erscheint, wenn die Beheizung der wärmeren Wand hinreichend stark ist. Die Stärke und Form des Sekundärwirbels wird von der Grashof-Zahl, der Reynolds-Zahl und von geometrischen Parametern wie Rippenteilung, Rippenhöhe und Neigungswinkel des Kanals gesteuert. Aufgrund der ermittelten Geschwindigkeits- und Temperaturfelder werden zusätzlich die Werte für den Druckgradienten und den Gesamtwärmeübergang innerhalb des Lösungsbereiches berechnet und dargestellt. Mittlerweile wird auch das Phänomen der auftriebsgesteuerten Strömungsumkehr in unberippten Kanälen diskutiert. Die Form der Strömungsumkehr in berippten und unberippten Kanälen erweisen sich als sehr unterschiedlich.

ВЛИЯНИЕ ПОДЪЕМНОЙ СИЛЫ НА ТЕПЛОВУЮ КОНВЕКЦИЮ В ВЕРТИКАЛЬНЫХ ОРЕБРЕННЫХ КАНАЛАХ ПРИ НИЗКИХ ЧИСЛАХ РЕЙНОЛЬДСА

Аннотация—Численно исследуется влияние подъемной силы на картину течения и теплоперенос в асимметрично нагреваемом канале с рядом теплопроводящих ребер. Ребра прикреплены к более нагретой стенке на одинаковых расстояниях в направлении течения, так что в развитой области преобладает течение периодического характера. Найдено, что в пределах одного модуля наряду с типичным рециркуляционным течением, имеющим место на задней поверхности ребра, у менее нагретой стенки возникает вторичный рециркуляционный вихрь при достаточно интенсивном нагреве более нагретой стенки. Установлено, что интенсивность и структура вторичного вихря определяются числами Грасгофа и Рейнольдса, а также такими геометрическими параметрами как расстояние между ребрами, высота ребра и угол наклона канала. На основе полученных решений для скорости и температуры определяются значения градиента давления и суммарного теплопереноса. Обсуждается также явление обращения потока за счет подъемной силы в неоребренном канале. Обнаружено большое различие между картиной обращения потоков в оребренных и неоребренных каналах.